

Recent Achievements and Future Challenges in Nanoscience and Nanotechnology

Z.A. Mansurov

Institute of Combustion Problems, 172 Bogenbay Batyr str., Almaty, Kazakhstan

Article info

Received:
20 January 2020

Received in revised form:
28 March 2020

Accepted:
5 May 2020

Abstract

The article presents the investigation results of the formation and synthesis of nanosized materials that were obtained at the Institute of Combustion Problems (ICP), many works have been brought to practical use. Investigations of low-temperature soot formation become the basis of nanomaterial synthesis methods, developed at the ICP since 1985. Below is a list of works on nanomaterials synthesis carried out at the Institute: a complete scheme of soot formation; a developed method for synthesis of nanocarbon, containing few layer graphenes from rice husk and walnut shell; the addition of 1.0% of activated carbon accelerates the burning rate of hydroxyl ammonium nitrate three times; also this activated nanocarbon is used as membranes for desalination of water up to 95%; perovskite photocatalysts based on SrTiO₃ and CoTiO₃/PAN fibers are used for hydrogen evolution reaction for sunlight illumination; obtaining carbon fibers by the method of electrospinning from coal tar pitches; obtaining of biologically soluble membranes based on polymeric nanofibres and hydroxyapatite of calcium.

1. Introduction

The article presents the investigation results of formation and synthesis of nanosized materials which were obtained at the Institute of Combustion Problems (ICP), a number of works have been brought to practical use. Investigations of low-temperature soot formation become the basis of nanomaterial synthesis method developed at the ICP since 1985 [1–3]. These studies are dedicated to low-temperature, cool-flame and soot-formation hydrocarbon flames.

Smalley in his famous article [4] noted 10 urgent problems associated with the development of mankind. Among them are clean air, clean water, energy, health. Fundamental and applied research is carried out in these areas at the ICP. This paper presents the results of this research obtained by our scientists during the last 5 years.

The indicated works were carried out under the projects of the Ministry of Education and Science of the Republic of Kazakhstan. We should note a wide

international cooperation within Ph.D. students preparation with the participation of foreign scientists as co-leaders, as well as holding International Symposium on Combustion and Plasma Chemistry and Carbon Materials and Nanoengineering, which made it possible to use foreign scientific and scientific and technical experience. The ultimate goal of basic research is the development of technology for producing nanomaterials and their practical use.

The appearance of the term «nanotechnology» is associated with the name of Japanese scientist N. Taniguchi (1974): «nanotechnology mainly consists of separation, consolidation and deformation processes of the materials, atom by atom or molecule by molecule». Nanotechnology is a set of methods, the result of which is the creation of technological chains for industrial production of nanomaterials with unusual properties, as well as various products obtained on their basis [5]. Currently, some developments (nanocarbon sorbents for water purification, hydroxyapatite, sponge – oil/water separation) have been brought to practical use, and prototypes have been made. The output of water purification devices is launched.

*Corresponding author. E-mail: zmansurov@kaznu.kz

TiO₂ and its derivatives are widely used in the production of photocatalysts, which may be utilized in hydrogen evolution and dye degradation areas [6–11]. Perovskite wide-gap semiconductors, mainly presented by SrTiO₃ and its doped modifications with a cubic structure are of great interest due to their strong catalytic activity, high chemical stability and long lifetime of electron-hole pairs [12–20].

The problem of the desalination of sea and ocean water is aggravated by the fact that the population of the planet is increasing rapidly (more than 80 million people per year) and by 2025 at least 2 billion people on the planet will systematically experience an acute shortage of fresh water [21–25]. Note also that fresh water is used differently by people in different countries. Fresh water consumption can go from 380 l per person per day in some countries to about 19 l per person per day in others. All these circumstances indicate that there is a problem with fresh water, and the need for water will only grow.

Desalination is a technology and a process that removes most of the salts from salt water [26]. The utilization of membranes increases significantly every year [25], and they have been subjects of very recent reviews [27–31]. The development of nanotechnologies and nanomaterials makes it possible to improve the structure and properties of water-permeable membranes. Carbon nanotubes, graphene materials and metal-organic framework compounds have had a significant impact on the permeability flux of the reverse osmosis membrane [32–37].

The new «era» of science throughout the world was marked by the discovery of nanomaterials. Carbon fibers have become materials that are of great technological and industrial importance due to the unique chemical, electrical, magnetic and mechanical properties. Carbon fibers are a form of carbon, formed predominantly by carbon atoms, consisting of thin filaments with a diameter of several microns. Carbon atoms are combined into microscopic crystals aligned parallel to each other, which gives the fiber greater tensile strength. Nowadays carbon fiber is one of the important engineering materials with great physicochemical and mechanical properties, which has various practical applications [38–40].

In modern medical practice in the field of surgery and dentistry to replace or repair damaged areas of bone tissue, materials based on calcium phosphates are widely used. Calcium phosphates are the most important inorganic components of

biological solid tissues. Hydroxyapatite calcium (HAP) is present in the composition of bone tissue, teeth and tendons, it gives the functionality and the necessary structure of the organs [41–44].

The treatment of various injuries and medical diseases often entails surgical intervention. Bone fractures are usually treated with metal plates, joints are replaced with artificial endoprostheses (thigh or knee), and lost teeth are replaced with metal implants. Phosphates of calcium have excellent biocompatibility, that is, they are practically not rejected by the human body. This depends on the fact that calcium phosphates are present in the human body in the dissolved or solid form [45, 46]. Calcium phosphates are used as a substitute for bone in orthopedics for the treatment of bone defects and dentistry. The ideal implant is, the patient's spongy bone, mixed with the plasma of his blood, is not available in sufficient quantities, then completely synthetic materials are used. Synthesized materials must undergo sterilization, which should not affect the biological properties of the substitute. Today, chemically synthetic materials are used to replace bones based on HAP and its composites [47, 48]. Crystalline hydroxyapatite can be synthesized in various ways, among which solid-phase synthesis methods are distinguished. Most often the synthesis of calcium phosphates is carried out from aqueous solutions using the processes of hydrolysis and precipitation.

2. Full scheme for soot, fullerenes and graphene formation in rich fuel flames

On the basis of the new data on the synthesis of fullerenes, carbon nanotubes, superhydrophobic soot and graphene in the flame it is possible to modify the general scheme proposed by H. Bockhorn for rich fuel flames [49]. We introduced a pressure-coordinate, which allows explaining the formation of fullerenes at low pressures. This scheme describes the formation of soot for different (any) types of fuel [50, 51]. Full scheme for soot, fullerenes and graphene formation in flames was developed by Z.A. Mansurov and recently published in [51].

3. Energy intensive nanocarbon materials

The usage of graphene oxide structures as energy-intensive additives can be one of the promising ways in order to increase the efficiency of high-energy rocket fuels. The interest is to use double-layered and multilayered graphene structures as such additives. A promising, simple and cost-effective

way are to obtain multilayered graphenes from rice husks (RH) and walnut shells (WS). At the Institute of Combustion Problems, a method for synthesis of multilayered graphene oxide structures (graphene oxide frameworks (GOFs)) from plant wastes such as rice husks or walnut shells [49–50] has been developed.

BET analysis of treated samples was carried out. Standard calculations for determining specific surface by BET method of carbonized rice husk and walnut-shell before activation showed that the specific surface of the samples is from 270 to 350 m²/g. As a result of the studies, it was found that the optimal temperature for thermochemical activation is 850 ± 5 °C and the activation time is 90 min. Under these conditions, there is formed a carbon material having a specific surface area of 2800 m²/g (walnut-shell), 4300 m²/g (rice husk), with a specific pore volume of – 1.1–1.8 cm³/g and average pore size of 2.6–1.7 nm. Chemically activated carbonized rice husk has a more developed specific surface area and a higher specific porosity in comparison with walnut-shell. The resulting carbon material has outstanding parameters of a specific surface area of about 4300 m² per gram, which is comparable to the specific surface area of metal-organic structures [52].

As a result of the carried out studies, a technique for getting graphene layers in accordance with the technology described in [53, 54] was developed. It is known that Raman spectroscopy is an informative method for studying graphene [55]. In this work, the number of graphene layers obtained from rice husk and walnut-shell is determined by Raman spectroscopy methods. This technique allows estimating the number of graphene layers, as well as the presence of chemical impurities, and structural defects in graphene (Fig. 1).

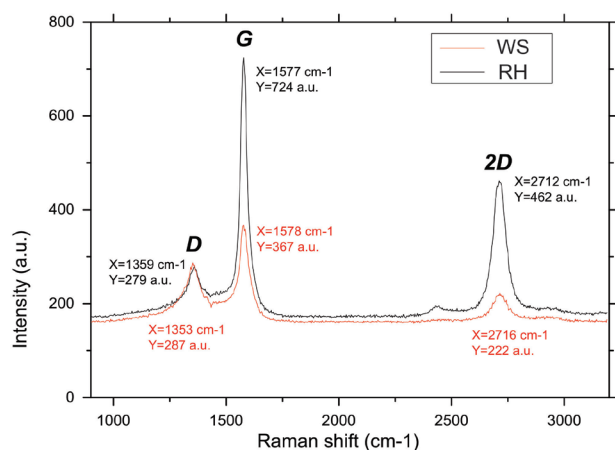


Fig. 1. Raman spectra of graphene obtained from rice husk and walnut-shell.

Table
Values of intensity ratio of I_D, I_G and I_{2D} for multilayered graphenes

#	I _D /I _G	I _{2D} /I _G	Note
1	0.85	0.05	Graphenes are not formed
2	1.5	1	2-layered graphenes
3	1.29	0.55	5- layered graphenes
4	1.16	0.58	4-layered graphenes
5	0.62	0.65	3-layered graphenes

Raman spectroscopy is a universal method for the identification of carbon nanomaterials. In [52], a method of determining the number of graphene layers according to peak intensities I_D, I_G and I_{2D} and their ratios, respectively. The data on determining the number of layers are presented in Table.

The Raman spectra of graphenes obtained from rice husk showed that the intensities of G and 2D peaks indicate that graphene film consists of regions with four or more layers (I_G/I_{2D} = 1.57 and I_D/I_G = 0.39). Spectral analysis of graphene obtained from walnut-shell: the intensities of G and 2D peaks indicate that the film consists of regions with multilayers (I_G/I_{2D} = 1.65 and I_D/I_G = 0.78). The Raman spectra of 2D distribution indicate that the formed structure is largely composed of multilayered graphenes. All spectra contain D, G, and 2D peaks, indicating the presence of deformations in the crystalline structure of graphene film, as well as mechanical stresses. A detailed observation of Raman spectroscopy showed that the samples obtained from rice husks and walnut shells consisted of graphene layers with amorphous components.

An influence of activated carbons with multilayered graphenes (three or more layers) on thermal decomposition of composition based on hydroxylammonium nitrate and carboxymethyl cellulose was investigated by differential thermal analysis method. It is shown that the addition of activated carbon with multilayered graphenes leads to an increase (four times) in the burning rate of hydroxylammonium nitrate. It was found that the temperature and time of a chemical reaction are reduced to complete decomposition of ammonium nitrate when activated carbon is added during thermal decomposition.

As a result of experiments (Fig. 2a), it was found that the addition of activated carbon into HAN/CMC mixture increases the combustion rate of composition (almost four times): in the mixture without coal, r_b = 13 mm/s at p₀ = 5 MPa, then as in mixture with coal r_b = 41 mm/s at p₀ = 5 MPa.

It is obvious that activated carbon will simulate a combustion reaction of the two-component composition of HAN/CMC. If the combustion of HAN/CMC mixture begins only at $p_0 = 3$ MPa, in the presence of 1% (from total mass) of activated carbon, the combustion begins already at $p_0 = 1$ MPa. Combustion of samples is accompanied by a bright flame with the release of a large amount of orange smoke (nitrogen dioxide). The combustion of HAN is accompanied by the formation of a large volume of gases, consisting mainly of NO, NO₂ and N₂O [56]. In rocket technology, such substances as HAN are used in gas generators in order to create excess pressure. Activated carbon and multilayered graphenes have many reactive centers on the surface in the form of pores and defects, free atoms at corners and faces, and are also characterized by a large specific surface. It is believed that on structural irregularities, defects and pores of carbon, activated centers are formed

that promote chemical processes. It can be assumed that during decomposition of NGAs in the presence of activated carbons, only in these centers there occurs heat accumulation, which in turn, raises the temperature of the entire system. The above mentioned factors play a role in the increase of oxidation rate as well as combustion fuel rate [54].

The combustion scheme of HAN with an addition of activated carbon in the liquid phase at $p_0 = 6$ MPa is shown in Fig. 2b. The process is characterized as convective combustion, incidental to the combustion of most single-component liquid fuels. In the presence of activated carbon, the combustion proceeds more rapidly, forming a turbulent flame, and a large volume of gases is released. The combustion process occurs in three zones (liquid – mixed zone, bubbles and gas-gas). It is assumed that during this process, the activated carbon particles are located inside fuel bubbles, which are formed upon heating of HAN, where a large amount of heat is accumulated due to the chemical reaction of fuel decomposition [56].

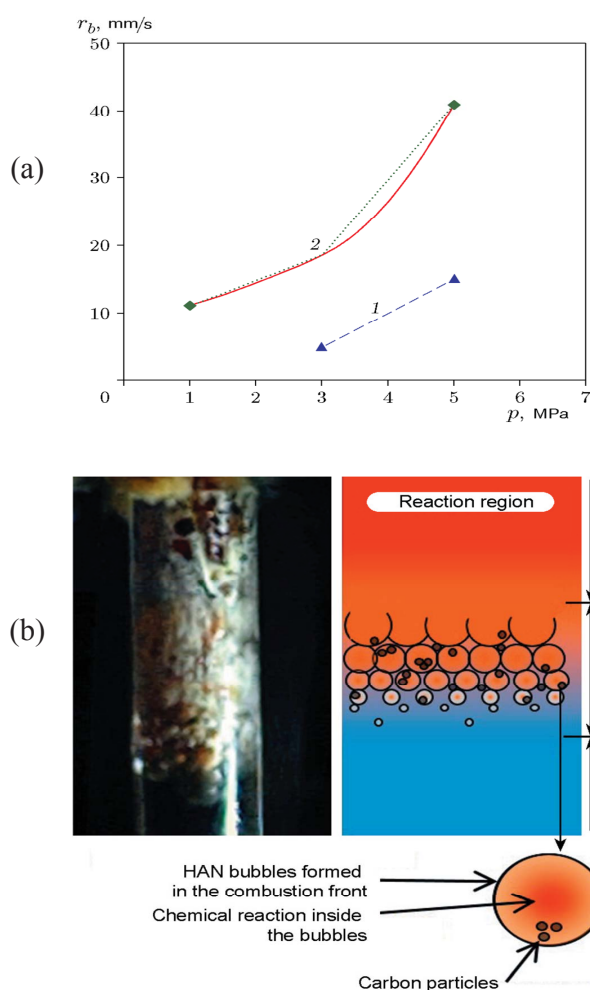


Fig. 2. a – Calculation of linear combustion rate of studied compositions depending on initial pressure system: 1 – HAN/CMC, 2 – HAN/CMC + activated carbon; b – combustion wave propagation at burning of HAN in liquid phase at $p_0 = 6$ MPa.

4. Synthesis of nanocarbon sorbents for purification of water from heavy metal ions

Membranes based on GO were prepared by vacuum filtration method [53]. First of all, the GO powder was mixed in deionized water and sonicated for 2 h. Then, 40 mL of the resulted GO suspension was separated through the membrane. Filtration processes performed under a vacuum atmosphere (-0.8 bar). The resultant membrane based on GO was dried under vacuum (-0.95 bar).

The GO membranes fluxes and rejections of five salt liquids were tested by a usual filtration system at room temperature. The solution volume was 200 mL. The filtration pressure was controlled and provided by a pump. The fabricated membranes were used for each filtration test. To check the repeatability of our method of making membrane, the stable flux of deionized water was measured and compared between different membrane samples (Fig. 3).

The desalination properties of membranes were tested for NaCl, KCl, MgCl₂, CaSO₄ and MgSO₄ using a calibrated Atomic Absorption Flame Emission Spectrophotometer. The initial composition of the salt (35 g/L) solution (sample of seawater) was as follows: NaCl (78.8%), KCl (2.1%), MgCl₂ (9.1%), CaSO₄ (3.5%) and MgSO₄ (6.5%).

The concentration of salts before and after filtration is shown in Fig. 4. The initial concentration of salts were: NaCl – 27.3 g/L, KCl – 0.7 g/L,

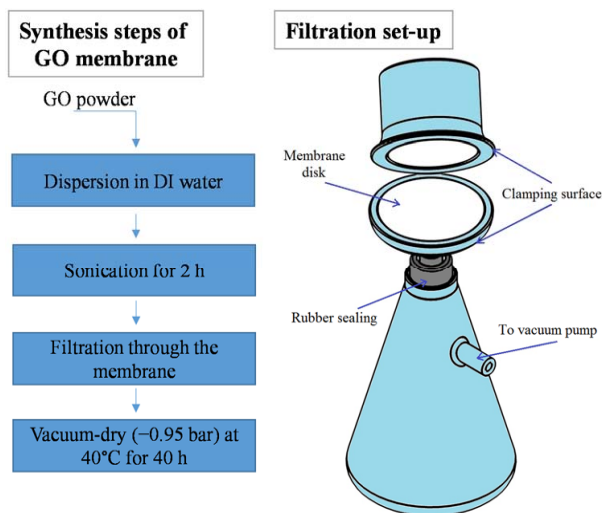


Fig. 3. The scheme of synthesis steps of GO membrane and filtration set-up.

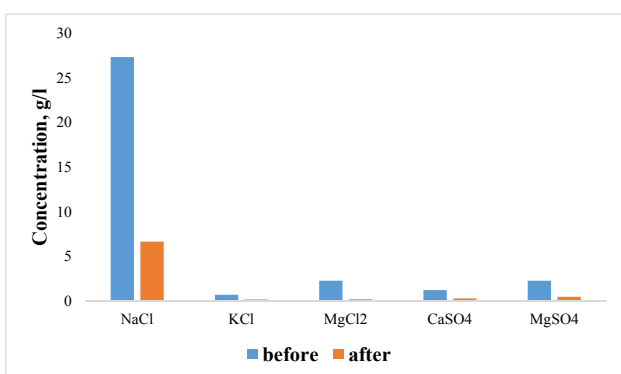


Fig. 4. Concentration of salts before and after filtration.

MgCl₂ – 2.275 g/L, CaSO₄ – 1.225 g/L and MgSO₄ – 2.275 g/L. After filtration of this solution through GO membranes, the concentration of salts decreases up to: NaCl – 6.64 g/L, KCl – 0.18 g/L, MgCl₂ – 0.19 g/L, CaSO₄ – 0.28 g/L and MgSO₄ – 0.46 g/L. From the obtained results, we can infer that permeability plays a crucial role in salt rejection: a slower process corresponds to a better filtration capability. In addition, the desalination of salt water with GO membranes makes it clear that the preparation of membranes from graphene oxide by vacuum filtration is more effective.

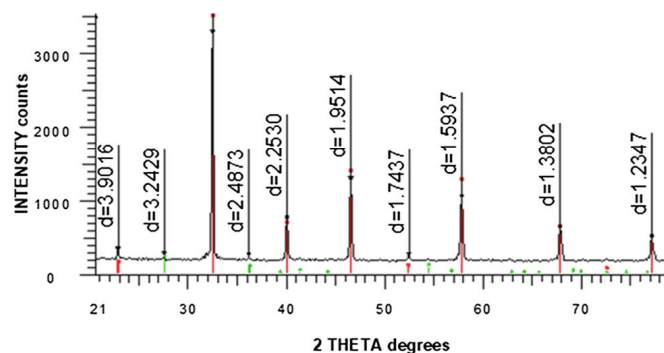
This study deals with the separation performance of salts through different kinds of membranes based on graphene. GO membranes were prepared by the vacuum filtration method. The desalination properties of GO membranes were successfully tested for the following salts: NaCl, KCl, MgCl₂, CaSO₄ and MgSO₄. According to the Atomic Absorption Flame Emission Spectrophotometry, the GO membranes can desalinate salt water up to 95%.

5. Development and study of perovskite photocatalysts for hydrogen evolution

The authors [57] obtained a composite 1D photocatalyst based on SrTiO₃/PAN fibers with strong alignment via the electrospinning technique. As a photocatalytic material SrTiO₃ with the particle size from 100 up to 350 nm was obtained by combined chemical solution and solid-state reaction method [58]. The obtained SrTiO₃ with the purity of 97% (Fig. 5a) was presented by spheroidal particles with numerous surface pores (Fig. 5b).

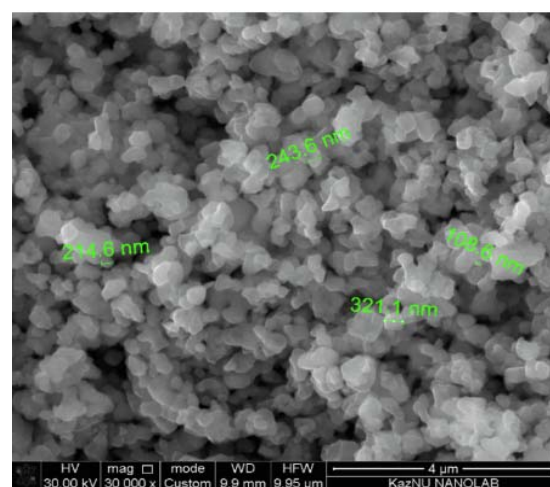
The electrospun 1D photocatalyst based on SrTiO₃/PAN is presented by fibrous highly oriented fibers with an average diameter of 2–4 microns. SrTiO₃ is distributed along with the structure of fibers, which is also verified by EDS analysis (Fig. 6a, b).

Photocatalysts based on SrTiO₃/PAN exhibited high activity in the splitting of water-methanol mixtures under 40W UV radiation with the highest yield of hydrogen 305 μmol h⁻¹ g⁻¹. Further, the activity of these 1D composite photocatalysts based on SrTiO₃/PAN was enhanced by the addition of



■ SrTiO₃
▲ TiO₂-Rutile

(a)



(b)

Fig. 5. X-ray pattern (a) and SEM (b) of the synthesized SrTiO₃ powder. This figure is reprinted from [57], with permission from Elsevier, 2019.

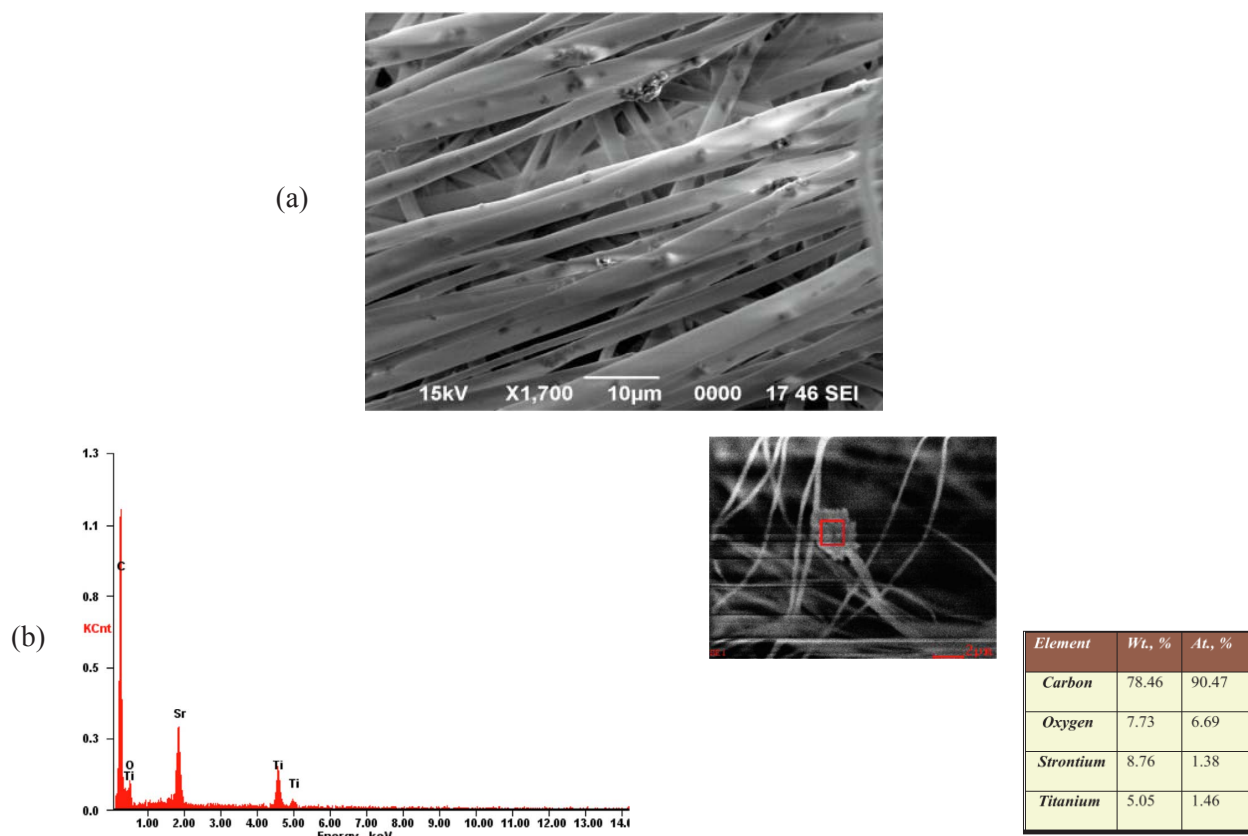


Fig. 6. SEM (a) and EDS (b) of aligned SrTiO₃/PAN based fibers. This figure is reprinted from [57], with permission from Elsevier, 2019

metal oxide particles, which are able to narrow the value of their bandgap [59]. The addition of Cr₂O₃, CuO, and Fe₂O₃ particles resulted in the bandgap decrease of the composite photocatalysts to 2.89, 2.84 and 3.11 eV, respectively (Fig. 7). Moreover, the yield of hydrogen under photocatalytic decomposition of the water-methanol mixture increased to 344.67 µmol h⁻¹ g⁻¹ for SrTiO₃/PAN/Fe₂O₃, 398.3 µmol h⁻¹ g⁻¹ for SrTiO₃/PAN/Cr₂O and 420.82 µmol h⁻¹ g⁻¹ for SrTiO₃/PAN/CuO based photocatalysts.

In [60], the authors proposed the formation of multilayered 3D photocatalyst based on CoTiO₃ with a multilayered structure by mixing Co₃O₄ and TiO₂ powders with the addition of a pore-forming agent. The calcined at different temperatures Co₃O₄ photocatalysts are presented by a multilayered structure with different porosity. In SEM images presented in Fig. 8 it can be seen that the pore size and microstructure of CoTiO₃ – based photocatalysts strongly depend on the calcination temperature. The specific surface area of the

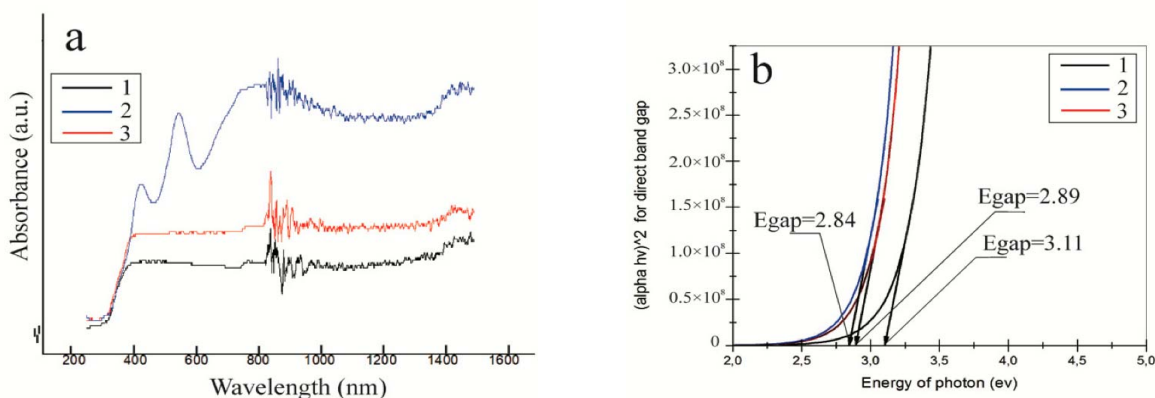


Fig. 7. Absorption and reflection spectra (a) and values of the bandgap (b) of synthesized composite photocatalysts: SrTiO₃/PAN/Fe₂O₃ – 1 (black line); SrTiO₃/PAN/CuO – 2 (blue line); and SrTiO₃/PAN/Cr₂O₃ – 3 (red line). This figure is reprinted from [59], with permission from MDPI, 2020.

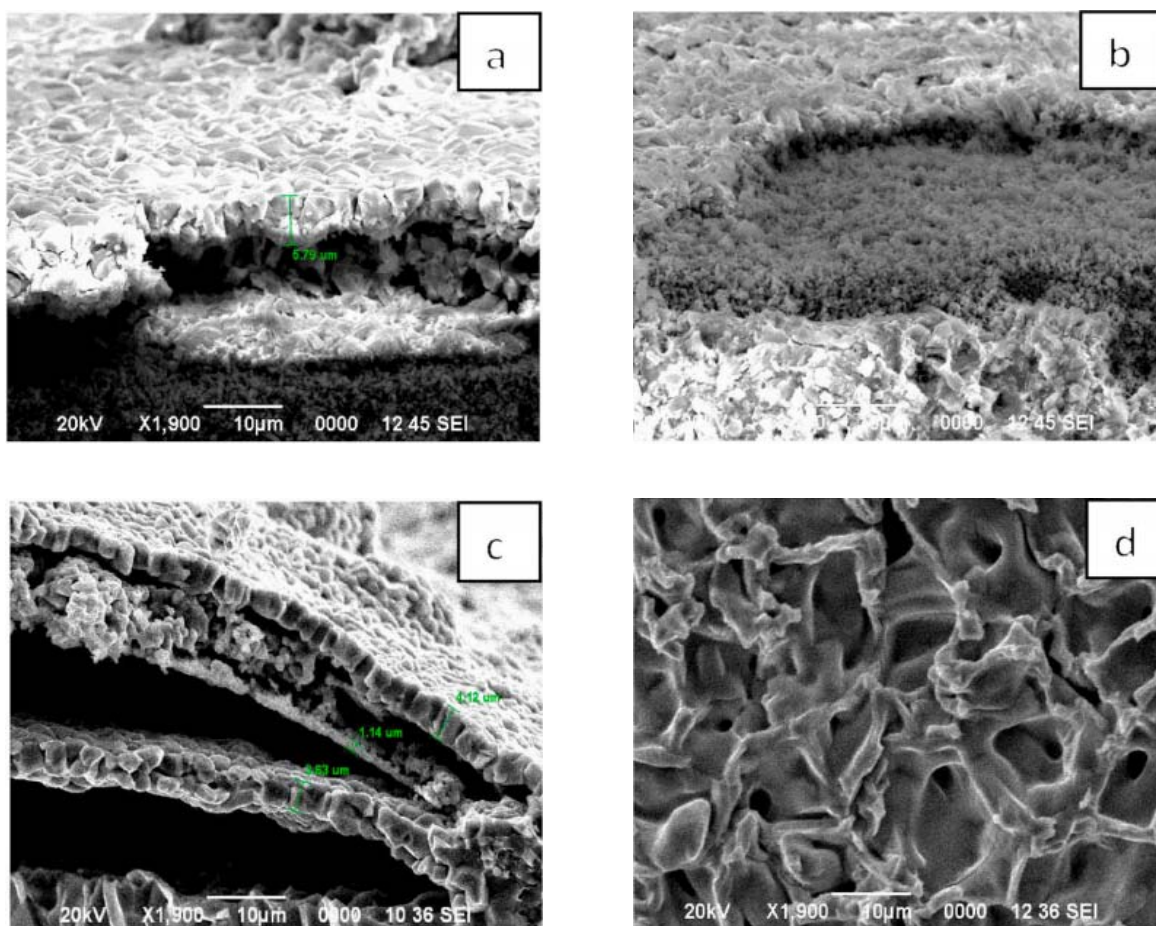


Fig. 8. SEM images of porous CoTiO_3 calcined at: a – 600 °C, b – 650 °C; c – 700 °C; d – 800 °C. This figure is reprinted from [60], with permission from Elsevier, 2021.

initial Co_3O_4 was nearly $14.71 \text{ m}^2/\text{g}$, while its value with the addition of 20% proppant increased to $29.23 \text{ m}^2/\text{g}$.

The I-V curves for photocatalysts based on CoTiO_3 calcined at 600 °C and 800 °C in dark and light conditions are almost the same, indicating that the presence or absence of light changes the structure of CoTiO_3 (Fig. 9). The investigated photo-response by the drop of initial voltage makes it possible for hydrogen evolution reaction to occur under the lower potential for the sunlight illumination.

Thus, high sintering temperature enhances the crystallinity and orientation of the photocatalyst, which leads to formation of an intermediate hyper-phase, providing more efficient separation of charge and increasing the efficiency of hydrogen evolution. The resulting photoanode based on CoTiO_3 exhibited the yield of hydrogen evolution from 0.5 M KOH solution of $0.3 \mu\text{mol h}^{-1} \text{g}^{-1}$ under the 40W mercury lamp and $0.024 \mu\text{mol h}^{-1} \text{g}^{-1}$ under xenon lamp.

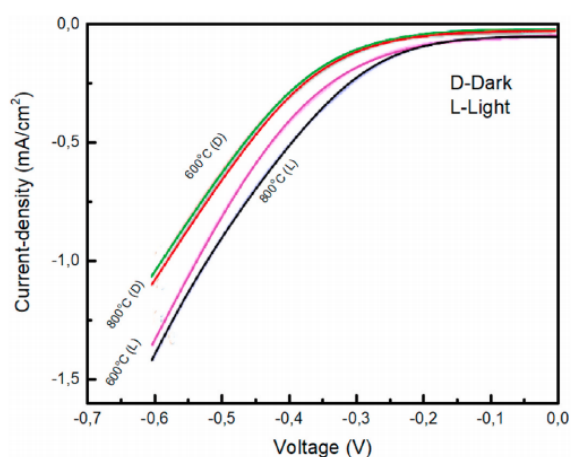


Fig. 9. I-V curves of porous CoTiO_3 in 0.5 M KOH solution.

6. Obtaining carbon fibers by the method of electrospinning

Electrospinning is a technique that allows fabrication of continuous fibrous materials with diameters down to a few nanometers. Electrospinning

is an electrostatically driven method of obtaining polymer and carbon fibers, such as PAN-based, pitch-based, lignin-based etc. Electrospinning is generally includes two modes of jet movement upon the jet emitting from the Taylor cone; a section of a stable jet in a straight line (short distance) followed by the essential and multiple vortex motion. A large number of works in the field of electrospinning are devoted to the development of collectors with various configurations: drum collectors (rotating), parallel electrodes and water baths. The main parameters of electrospinning are the speed of movement of the collecting surface of the collector, the effect of the electric field. To obtain carbon fibers by electrospinning, an installation was developed, the general scheme of which is shown in Fig. 10.

At first glance, electrospinning appears to be a simple and therefore easily controllable fiber production method. But this process is complex and depends on numerous factors. The use of the required precursor and its preparation are fundamental steps in the production of fibers. The use of a rotating collector in an electrospinning machine is the earliest method for producing oriented fibers. Not all materials can be used with a rotating collector in the electrospinning process. Fibers produced by electrospinning from a brittle material must break at a lower rotational speed than a flexible or elastic material. The method with a rotating collector is time/energy intensive. Fiber alignment is usually very low and decreases with increasing spinning time and fiber material thickness.

It was found that the alignment of the fibers increases with an increasing surface speed of the

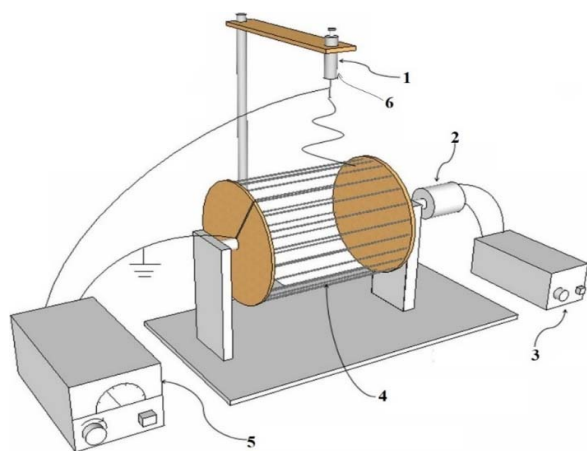


Fig. 10. General diagram of the electrospinning installation: 1 – syringe; 2 – motor; 3 – motor speed controller; 4 – drum collector; 5 – high-voltage power supply; 6 – needle.

drum to a critical value. The resulting fibrous materials can be divided into three stages depending on the rotational speed of the collector: the rotation speed is too low to ensure fiber orientation; rotation initiates fiber alignment; fiber alignment is reduced due to turbulent air flow around the rotating manifold at the critical rotation speed.

The collector rotation speed affects the fiber diameter, which is inversely proportional to the rotation speed. An increase in the rotational speed of the collector leads to a decrease in the fiber diameter.

Petroleum pitch can be obtained from heavy oil residues obtained in the catalytic cracking process, tar – a by-product of steam cracking of naphtha, gas oil, or any residues from the distillation or refining of oil. Many methods can be used to produce a pitch and are based on refining processes:

1. Heat treatment to advance the molecular weight of the components.
2. Air bowing.
3. Steam stripping and application of vacuum to remove low boiling components.
4. Distillation.

The chemical and physical characteristics of petroleum pitch depend on the process and conditions used (process temperature and heat treatment time). Longer times and higher temperatures result in pitch with increased aromaticity and higher anisotropy. Petroleum pitches are generally less aromatic than coal tar pitch.

Coal tar is a by-product of coking coal in the production of coke. Metallurgical coke is produced at high temperatures (900–1100 °C), smokeless fuels are produced at lower temperatures (600 °C). The low-temperature process produces less resin than the high-temperature process. In the process of distillation and heat treatment, coal tar pitch is obtained from coal tar. Resin is the residue that remains after the removal of heavy oil fractions (creosote or anthracene). Resin is a complex mixture containing many different individual organic compounds, the composition and properties depend on the source of the resin and the method of processing. Two thirds of the compounds isolated from coal tar pitch are aromatic, and the rest is heterocyclic. Most of the components of coal tar pitches contain three to six rings with boiling points in the range of 340–550 °C.

The technological scheme of obtaining carbon fibers based on pitches consists of the following stages:

1. Raw material preparation in a quartz furnace (200–500 °C, 2 h, argon);

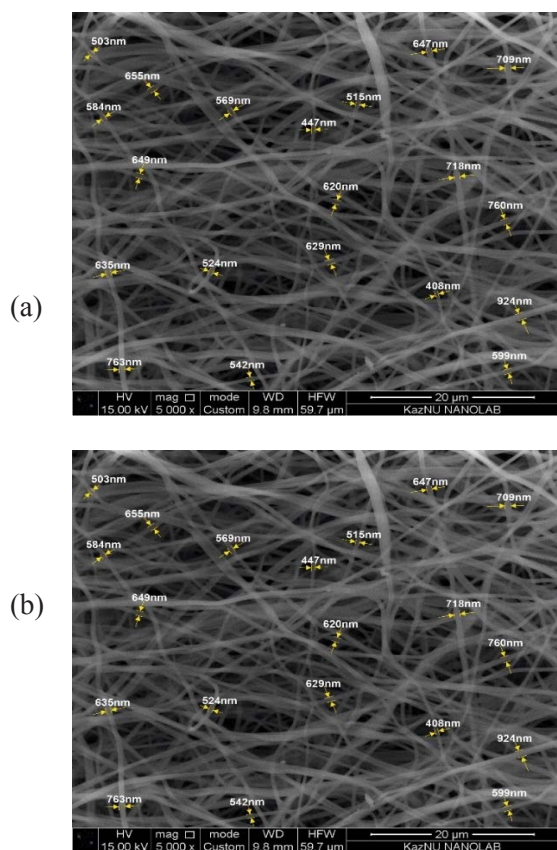


Fig. 11. SEM images of samples of carbon fibers based on coal tar pitches and PAN (a) after stabilization and (b) after carbonization.

2. Cooling and material collection;
3. Preparation of solutions with the addition of PAN;
4. Electrospinning process;
5. Stabilization of the obtained fibers in a quartz reactor in an oxygen atmosphere (at a temperature 250–280 °C of 1 h) and carbonization in a quartz reactor under an argon atmosphere (at a temperature 500–600 °C of 1 h).

In the SEM images (11) it can be seen that after the carbonization process, thinner and smoother fibers are formed in all samples, this is because all volatile substances evaporate under the influence of temperature. The property of preservation of fibrous structures in all samples is also noted, which is explained by the influence of the formation of mesophase centers in the fiber structure.

7. Obtaining of biologically soluble membranes based on polymeric nanofibres and hydroxyapatite of calcium

Synthetic HAP (hydroxyapatite) was obtained from biological waste material. The egg shell containing CaCO_3 is annealed for 2 to 3 h at a tem-

perature of 900–1000 °C. During annealing, the organic component of the shell burns off, and the resulting residue contains CaO as a fine powder without impurities. As a result, crystals with a size of 1–2 microns are formed. It is worth to note that studies of the obtained crystalline calcium hydroxyapatite, show that external conditions such as pH, composition and concentration of reagents and impurities, order and speed of mixing, temperature, time of the experiment strongly affect the crystallization process and the chemical composition of the synthesized powder. The resulting powdered material is a micron-sized fine powder (1–2 μm).

Further synthesized HAP was subjected to post-thermal treatment at temperature 1100 °C in an air medium for 3 h to increase its crystallinity. The X-ray diffraction patterns of the HAP before post-thermal treatment (line 1) and after it (line 2) are presented in Fig. 12. The main diffraction peaks corresponding to the HAP are shifted toward smaller angles, and the interplanar spacing decreases, this indicating a high degree of crystallinity of post-thermal treated HAP (Fig. 12, line 2). Simultaneously, the broad peaks, indicating the heterogeneity of the structure and the presence of defects (Fig. 12, line 1), are observed in HAP's X-ray pattern without post-thermal treatment.

Structure imperfections due to the presence of vacancies, impurities of implementation and substitution, and determined by them distortions in the crystal lattice became energetically advantageous for the formation of HAP in the hexagonal syngony. Therefore, the presence of microimpurities and other defects in the structure of biological apatite

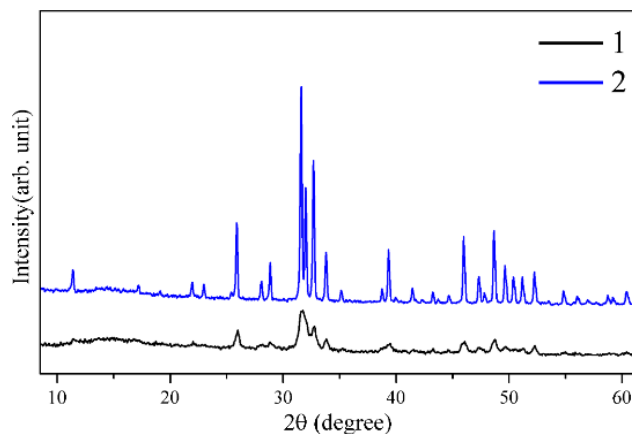


Fig. 12. X-ray diffraction patterns of HAP: 1 – HAP particles without post-thermal treatment; 2 – HAP particles with post-thermal treatment at a temperature of 1100 °C for 3 h.

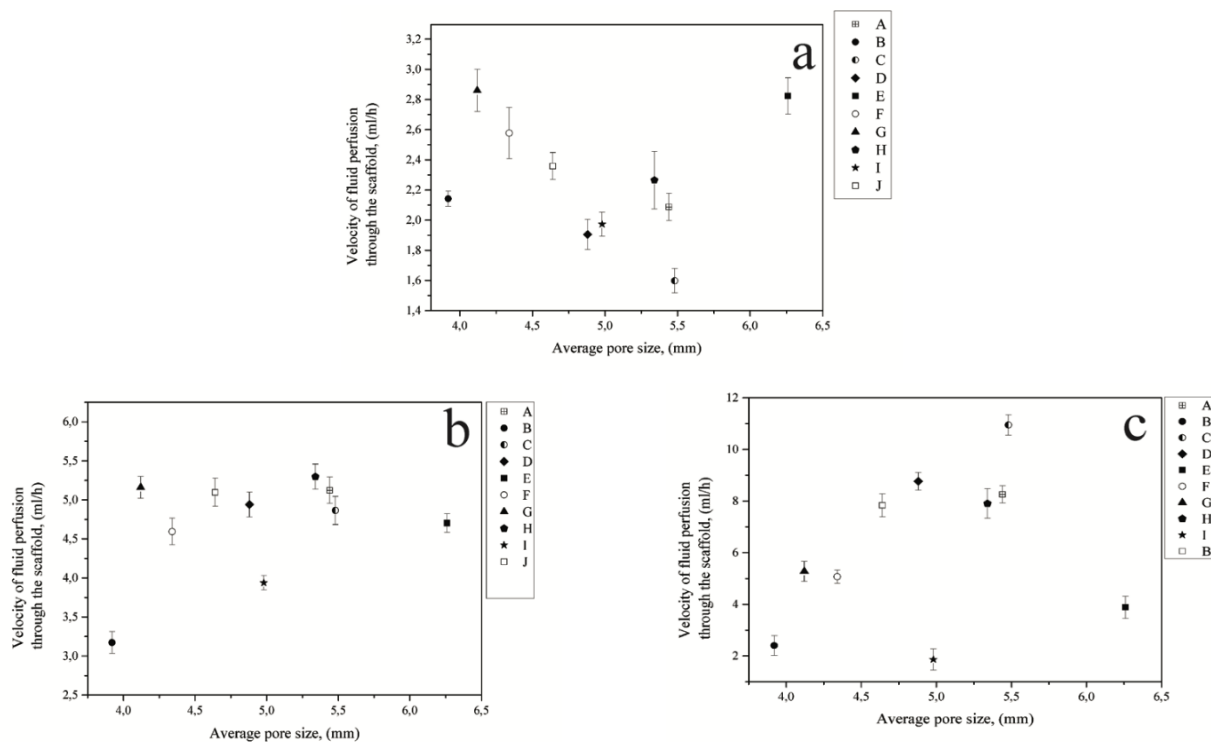


Fig. 13. Influence of the average pore size on the rate of diffusion of nutrient fluid through the scaffold at its rotation rate of 6 (a), 12 (b) and 24 (c) rpm.

determines its characteristics and affects the physico-chemical and chemical-biological properties. Atoms of impurity can be located randomly in the structure of hydroxyapatite [61]. To describe the structure of HAP, it is convenient to formulate the ideal stoichiometric formula of $\text{Ca}_{10}(\text{PO}_4)_6(\text{OH})_2$, taking into account the different positions occupied by calcium atoms in the lattice of HAP as $\text{Ca}_{10}(\text{PO}_4)_6(\text{OH})_2$, and also calculating the Ca/P ratio, which for our samples was 1.5. This feature is typical for the whole class of calcium apatites and can be considered using the example of a unit cell of the HAP (Fig. 13) [62].

The values of the rate of diffusion flow of nutrients depending on the average pore size of the scaffold, which is in the range from 3.92 to 6.26 mm at a certain rotation rate, showed that the geometric shape of the scaffold has a significant effect on the movement of the nutrient fluid. For the G and E scaffold, the average pore size is 4.12 and 6.26 mm, respectively, but for both scaffolds the rate of diffusion flow of nutrients is approximately the same – 2.8 ml/h (Fig. 13a). A detailed study of the effect of the average pore size of scaffolds on the rate of diffusion flow of nutrients through it at 12 rpm (Fig. 13 b) indicates that the pores do not significantly affect the rate of nutrient spread. Such behavior at similar parameters is confirmed in ex-

perimental works [63–65] and possibly indicates the selection of optimal scaffold rotation rate. At rotation rates of 24 rpm (Fig. 13c) and 6 rpm (Fig. 13a), the influence of the geometric shape on the distribution of the nutrient in the scaffold is clearly seen.

8. Conclusions

The results are summarized in this mini review in the fields of nanotechnologies and nanomaterials at the Institute of Combustion Problems. On the basis of previous investigations of the formation of fullerenes, graphenes and soot particles a full scheme of soot formation rich by fuel hydrocarbon flames is developed. A method for obtaining layer graphenes from rising husk was developed. Activated carbon with a large specific surface ($3000 \text{ m}^2/\text{g}$) containing 5–10% of multilayer graphene (three and more sheets: $I_{2D}/I_G = 0.63$) was obtained. It was experimentally found that the addition of activated carbon (1% of the total mass) to hydroxyl ammonium nitrate leads to a four-fold increase in the burning rate at the initial pressure of 5 MPa.

On the base of a few layers, graphenes from rice husk were prepared membranes for desalination. The desalination properties of membranes were successfully tested for the following salts: NaCl,

KCl, MgCl₂, CaSO₄ and MgSO₄. According to the Atomic Absorption Flame Emission Spectrophotometry, the GOM and GM membranes can desalinate salt water about 95%.

Multilayered 3D porous CoTiO₃ films with high specific surfaces area were sintered by mixing Co₃O₄, TiO₂ nanopowders with a pore-forming agent, and further calcination. CoTiO₃ film quality was investigated by SEM, XRD, BET, and optical measurement analysis. High calcination temperatures decrease the porosity of CoTiO₃ films and increase their crystal size at the same amount of agent adding. The results demonstrated in this paper show the advantages of using 3D porous CoTiO₃ as an active photocatalyst for producing hydrogen under sunlight illumination.

Spinnable pitch and carbon fibers were successfully prepared from coal tar as an alternative precursor with the addition of polymer. Carbon fibers were produced from the above pitch using the electrospinning method. Polymethylmethacrylate (PMMA) was solved in 1,2 – dichloroethane. The optimal ratio of PMAA/coal–tar was 50/50%.

It was found that HAP crystalline powder obtained by chemical precipitation from an aqueous solution using a biologically waste material – eggshell, has a purity of more than 95%. A distinctive feature of the existing methods for producing HAP, in this work, is post-thermal firing at a temperature of 1100 °C in the air for 2 h, which made it possible to obtain HAP particles with sizes up to 200 nm, as well as improve its crystal structure.

References

- [1]. Z.A. Mansurov, B.K. Tuleutaev, R.Kh. Salakhov, V.T. Popov, Yu. Korolev. Producing of soot formation in cold methane flame mode. Collection of works on chemistry. Alma-Ata, 1985. Issue 10. P. 158–163 (in Russian).
- [2]. Z.A. Mansurov, V.I. Pesterev, D.U. Bodykov. The use of low-temperature IR spectroscopy in study of cold flames. Abstracts of the scientific and practical seminar on combustion electrophysics. Karaganda, 1987, p. 103 (in Russian).
- [3]. Z.A. Mansurov, *Combust. Explos. Shock Waves* 48 (2012) 561–569. DOI: 10.1134/S0010508212050073
- [4]. R.E. Smalley, *MRS Bulletin* 30 (2005) 412–417. DOI: 10.1557/mrs2005.124
- [5]. N. Taniguchi, (1974) On the Basic Concept of Nanotechnology. Proceedings of the International Conference on Production Engineering, Tokyo, 18-23.
- [6]. A. Samokhvalov, *Renew. Sust. Energ. Rev.* 72 (2017) 981–1000. DOI: 10.1016/j.rser.2017.01.024
- [7]. T. Ye, W. Qi, X. An, H. Liu, J. Qu, *Sci Total Environ* 688 (2019) 592–599. DOI: 10.1016/j.scitotenv.2019.06.319
- [8]. C. Daulbayev, F. Sultanov, B. Bakbolat, O. Daulbayev, *Int. J. Hydrogen Energ.* 45 (2020) 33325–33342. DOI: 10.1016/j.ijhydene.2020.09.101
- [9]. T. Jose, C. Vincent, K.O. Lilly, M.A. Lazar. *Materials Today: Proceedings* 9 (2019) 21–26. DOI: 10.1016/j.matpr.2019.02.031
- [10]. W.K. Wang, W. Zhu, L. Mao, J. Zhang, Z. Zhou, G. Zhao, *J. Colloid Interf. Sci.* 557 (2019) 227–235. DOI: 10.1016/j.jcis.2019.08.088
- [11]. B. Bakbolat, C. Daulbayev, F. Sultanov, R. Beissenov, A. Umirzakov, A. Mereke, A. Bekbaev, I. Chuprakov, *Nanomaterials* 10 (2020) 1790. DOI: 10.3390/nano10091790
- [12]. C. Collignon, X. Lin, C.W. Rischau, B. Fauqué, K. Behnia, *Annu. Rev. Condens. Ma P.* 10 (2019) 25–44. DOI: 10.1146/annurev-conmatphys-031218-013144
- [13]. B.L. Phoon, C.W. Lai, J.C. Juan, P.-L. Show, G.-T. Pan, *Int. J. Hydrogen Energ.* 44 (2019) 14316–14340. DOI: 10.1016/j.ijhydene.2019.01.166
- [14]. A. Mishra, A. Mehta, S. Basu, *J. Environ. Chem. Eng.* 6 (2018) 6088–6107. DOI: 10.1016/j.jece.2018.09.029
- [15]. B. Thomas, L.K. Alexander, *J. Alloy. Compd.* 788 (2019) 257–266. DOI: 10.1016/j.jallcom.2019.02.190
- [16]. M. Ahmadi, M.S. Seyed Dorraji, M.H. Rasoulifard, A.R. Amani-Ghadim, *Sep. Purif. Technol.* 228 (2019) 115771. DOI: 10.1016/j.seppur.2019.115771
- [17]. Y. Wu, T. He, *Spectrochim. Acta A* 199 (2018) 283–289. DOI: 10.1016/j.saa.2018.03.078
- [18]. D. Zhou, P. Zhai, G. Hu, J. Yang, *Chem. Phys. Lett.* 711 (2018) 77–80. DOI: 10.1016/j.cplett.2018.09.024
- [19]. D. Saadetnejad, R. Yildirim, *Int. J. Hydrogen Energ.* 43 (2018) 1116–1122. DOI: 10.1016/j.ijhydene.2017.10.154
- [20]. L. Hu, X.-W. Yan, X.-J. Zhang, D. Shan, *Appl. Surf. Sci.* 428 (2018) 819–824. DOI: 10.1016/j.apsusc.2017.09.216
- [21]. B.B. Tanganov, *Modern high technology* 7 (2010) 90–92.
- [22]. X. Zheng, J. Wen, L. Shi, R. Cheng, Z. Zhang, *Desalination* 488 (2020) 114523. DOI: 10.1016/j.desal.2020.114523
- [23]. J. Safaei, P. Xiong, G. Wang, *Materials Today Advances* 8 (2020) 100108. DOI: 10.1016/j.mtadv.2020.100108
- [24]. H. Saleem, L. Trabzon, A. Kilic, S.J. Zaidi,

- Desalination* 478 (2020) 114178. DOI: [10.1016/j.desal.2019.114178](https://doi.org/10.1016/j.desal.2019.114178)
- [25]. The United Nations World Water Development Report 2014: Water and Energy. Printed by UNESCO CLD, Paris. ePub ISBN 978-92-3-904259-3
- [26]. M. Elimelech, W.A. Phillip, *Science* 333 (2011) 712–717. DOI: [10.1126/science.1200488](https://doi.org/10.1126/science.1200488)
- [27]. S. Fang, W. Tu, L. Mu, Z. Sun, Q. Hu, Y. Yang, *Renew. Sust. Energ. Rev.* 113 (2019) 109268. DOI: [10.1016/j.rser.2019.109268](https://doi.org/10.1016/j.rser.2019.109268)
- [28]. Z. Yang, X.-H. Ma, C.Y. Tang, *Desalination* 434 (2018) 37–59. DOI: [10.1016/j.desal.2017.11.046](https://doi.org/10.1016/j.desal.2017.11.046)
- [29]. Y.H. Teow, A.W. Mohammad, *Desalination* 451 (2019) 2–17. DOI: [10.1016/j.desal.2017.11.041](https://doi.org/10.1016/j.desal.2017.11.041)
- [30]. Z. Li, A. Siddiqi, L.D. Anadon, V. Narayanamurti, *Renew. Sust. Energ. Rev.* 82 (2018) 3833–3847. DOI: [10.1016/j.rser.2017.10.087](https://doi.org/10.1016/j.rser.2017.10.087)
- [31]. A. Boretti, S. Al-Zubaidy, M. Vaclavikova, M. Al-Abri, S. Castelletto, S. Mikhalovsky, *npj Clean Water* 1 (2018) 5. DOI: [10.1038/s41545-018-0004-z](https://doi.org/10.1038/s41545-018-0004-z)
- [32]. X. Li, B. Zhu, J. Zhu, *Carbon* 146 (2019) 320–328. DOI: [10.1016/j.carbon.2019.02.007](https://doi.org/10.1016/j.carbon.2019.02.007)
- [33]. A.S. Kazemi, S.M. Hosseini, Y. Abdi, *Desalination* 451 (2019) 160–171. DOI: [10.1016/j.desal.2017.12.050](https://doi.org/10.1016/j.desal.2017.12.050)
- [34]. J. Farahbakhsh, M. Delnavaz, V. Vatanpour, *J. Memb. Sci.* 581 (2019) 123–138. DOI: [10.1016/j.memsci.2019.03.050](https://doi.org/10.1016/j.memsci.2019.03.050)
- [35]. I.W. Azelee, P.S. Goh, W.J. Lau, A.F. Ismail, *J. Clean. Prod.* 181 (2018) 517–526. DOI: [10.1016/j.jclepro.2018.01.212](https://doi.org/10.1016/j.jclepro.2018.01.212)
- [36]. Q. Li, D. Yang, J. Shi, X. Xu, S. Yan, Q. Liu, *Desalination* 379 (2016) 164–171. DOI: [10.1016/j.desal.2015.11.008](https://doi.org/10.1016/j.desal.2015.11.008)
- [37]. S. Hadadpour, I. Tavakol, Z. Shabani, T. Mohammadi, M.A. Tofighy, S. Sahebi, *J. Environ. Chem. Eng.* 9 (2021) 104880. DOI: [10.1016/j.jece.2020.104880](https://doi.org/10.1016/j.jece.2020.104880)
- [38]. J. Deng, L. Xu, J. Liu, J. Peng, Z. Han, Z. Shen, S. Guo, *Polym. Degrad. Stabil.* 182 (2020) 109419. DOI: [10.1016/j.polymdegradstab.2020.109419](https://doi.org/10.1016/j.polymdegradstab.2020.109419)
- [39]. J. Zhang, V.S. Chevali, H. Wang, C.-H. Wang, *Compos. Part B - Eng.* 193 (2020) 108053. DOI: [10.1016/j.compositesb.2020.108053](https://doi.org/10.1016/j.compositesb.2020.108053)
- [40]. J. Du, H. Zhang, Y. Geng, W. Ming, W. He, J. Ma, Y. Cao, X. Li, K. Liu, *Ceram. Int.* 45 (2019) 18155–18166. DOI: [10.1016/j.ceramint.2019.06.112](https://doi.org/10.1016/j.ceramint.2019.06.112)
- [41]. S.-L. Bee, Z.A.A. Hamid, *Ceram. Int.* 46 (2020) 17149–17175. DOI: [10.1016/j.ceramint.2020.04.103](https://doi.org/10.1016/j.ceramint.2020.04.103)
- [42]. S. Mondal, U. Pal, *J. Drug Deliv. Sci. Tec.* 53 (2019) 101131. DOI: [10.1016/j.jddst.2019.101131](https://doi.org/10.1016/j.jddst.2019.101131)
- [43]. M. Farokhi, F. Mottaghitlab, S. Samani, M.A. Shokrgozar, S.C. Kundu, R.L. Reis, Y. Fatahi, D.L. Kaplan, *Biotechnol. Adv.* 36 (2018) 68–91. DOI: [10.1016/j.biotechadv.2017.10.001](https://doi.org/10.1016/j.biotechadv.2017.10.001)
- [44]. M.N. Hassan, M.M. Mahmoud, A.A. El-Fattah, S. Kandil, *Ceram. Int.* 42 (2016) 3725–3744. DOI: [10.1016/j.ceramint.2015.11.044](https://doi.org/10.1016/j.ceramint.2015.11.044)
- [45]. Md. Minhajul Islam, Md. Shahruzzaman, Shanta Biswas, Md. Nurus Sakib, Taslim Ur Rashid, *Bioactive Materials* 5 (2020) 164–183. DOI: [10.1016/j.bioactmat.2020.01.012](https://doi.org/10.1016/j.bioactmat.2020.01.012)
- [46]. Y.G. Lim, H.J. Kim, Jin Won Kim, Kyeongsoon Park, *J. Ind. Eng. Chem.* 89 (2020) 442–447. DOI: [10.1016/j.jiec.2020.06.018](https://doi.org/10.1016/j.jiec.2020.06.018)
- [47]. Ch. Daulbayev, Z. Mansurov, G. Mitchell, A. Zakhidov, *Eurasian Chem.-Tech. J.* 20 (2018) 119–124. DOI: [10.18321/ectj690](https://doi.org/10.18321/ectj690)
- [48]. S. Bayda, M. Adeel, T. Tuccinardi, M. Cordani, F. Rizzolio, *Molecules* 25 (2019) 112. DOI: [10.3390/molecules25010112](https://doi.org/10.3390/molecules25010112)
- [49]. Soot Formation in Combustion. Ed. H. Bockhorn, Heidelberg, Springer, 1994. P. 596. DOI: [10.1007/978-3-642-85167-4](https://doi.org/10.1007/978-3-642-85167-4)
- [50]. Z.A. Mansurov. Soot formation. Almaty: Kazakh University. 2015, 167 p.
- [51]. Z.A. Mansurov, *Eurasian Chem.-Technol. J.* 20 (2018) 277–281. DOI: [10.18321/ectj760](https://doi.org/10.18321/ectj760)
- [52]. Z.A. Mansurov, M.K. Atamanov, Zh. Elemesova, B.T. Lesbaev, M.N. Chikradze, *Combust. Explos. Shock Waves* 55 (2019) 402–408. DOI: [10.1134/S0010508219040051](https://doi.org/10.1134/S0010508219040051)
- [53]. M.A. Seitzhanova, D.I. Chenchik, S.K. Tanirbergenova, Z.A. Mansurov, *Combustion and Plasmachemistry [Gorenie i Plazmohimija]* 15 (2017) 248–253 (in Russian).
- [54]. J.M. Jandosov, N.V. Shikina, M.A. Bijsenbayev, M.E. Shamalov, Z.R. Ismagilov, Z.A. Mansurov, *Eurasian Chem.-Technol. J.* 11 (2009) 245–252. DOI: [10.18321/ectj287](https://doi.org/10.18321/ectj287)
- [55]. Umber Kalsoom, M. Shahid Rafique, Shamaila Shahzadi, Khizra Fatima, Rabia Shaheen, *Mater. Sci.-Poland* 35 (2017) 687–693. DOI: [10.1515/msp-2017-0099](https://doi.org/10.1515/msp-2017-0099)
- [56]. M.K. Atamanov, R. Amrousse, K. Hori, B.Ya. Kolesnikov, Z.A. Mansurov, *Combust. Explos. Shock. Waves* 54 (2018) 72–81. DOI: [10.1134/S0010508218030085](https://doi.org/10.1134/S0010508218030085)
- [57]. F. Sultanov, C. Daulbayev, B. Bakbolat, O. Daulbayev, M. Bigaj, Z. Mansurov, K. Kuterbekov, K. Bekmyrza, *Chem. Phys. Lett.* 737 (2019) 136821. DOI: [10.1016/j.cplett.2019.136821](https://doi.org/10.1016/j.cplett.2019.136821)
- [58]. P.K. Roy, J. Bera, *Mater. Res. Bull.* 40 (2005) 599–604. DOI: [10.1016/j.materresbull.2005.01.010](https://doi.org/10.1016/j.materresbull.2005.01.010)
- [59]. F. Sultanov, C. Daulbayev, S. Azat, K. Kuterbekov, K. Bekmyrza, B. Bakbolat, M. Bigaj, Z. Mansurov, *Nanomaterials* 10 (2020) 1734. DOI: [10.3390/nano10091734](https://doi.org/10.3390/nano10091734)

- [60]. R.E. Beissenov, A.L. Mereke, A.G. Umirzakov, Z.A. Mansurov, B.A. Rakhmetov, Y.Y. Beisenova, A.A. Shaikenova, D.A. Muratov, *Mat. Sci. Semicon. Proc.* 121 (2021) 105360. DOI: [10.1016/j.mssp.2020.105360](https://doi.org/10.1016/j.mssp.2020.105360)
- [61]. D.B. Lima, M.A. Araújo de Souza, G. Goetten de Lima, E.P.F. Souto, H.M.L. Oliveira, M.V. Lia Fook, M.J. Cavalcanti de Sá, *Carbohydr. Polym.* 245 (2020) 116575. DOI: [10.1016/j.carbpol.2020.116575](https://doi.org/10.1016/j.carbpol.2020.116575)
- [62]. Ch. Daulbayev, Z. Mansurov, F. Sultanov, M. Shams, A. Umirzakov, S. Serovajsky, *Eurasian Chem.-Technol. J.* 22 (2020) 149–156. DOI: <https://doi.org/10.18321/ectj974>
- [63]. E.A. Botchwey, S.R. Pollack, E.M. Levine, E.D. Johnston, C.T. Laurencin, *J. Biomed. Mater. Res.* 69A (2004) 205–215. DOI: [10.1002/jbm.a.10163](https://doi.org/10.1002/jbm.a.10163)
- [64]. L.V. Gonzalez Gil, H. Singh, J. de S. da Silva, D.P. dos Santos, D.T. Covas, K. Swiech, C.A. Torres Suazo, *Biochem. Eng. J.* 162 (2020) 107710. DOI: [10.1016/j.bej.2020.107710](https://doi.org/10.1016/j.bej.2020.107710)
- [65]. B.S. Borys, A. Le, E.L. Roberts, T. Dang, L. Rohani, C.Y.-M. Hsu, A.A. Wyma, D.E. Rancourt, I.D. Gates, M.S. Kallos, *J. Biotechnol.* 304 (2019) 16–27. DOI: [10.1016/j.jbiotec.2019.08.002](https://doi.org/10.1016/j.jbiotec.2019.08.002)